Fluid Dynamics & Materials Processing

Tech Science Press

DOI: 10.32604/fdmp.2024.052396

ARTICLE

Influence of Rayleigh-Taylor Instability on Impurity Dynamics during Column Back-Flushing Filtration

Yanina N. Parshakova* **and Andrey Ivantsov**

Institute of Continuous Media Mechanics, Ural Branch of the Russian Academy of Sciences, Perm, 614013, Russia

*Corresponding Author: Yanina N. Parshakova. Email: parshakova@icmm.ru

Received: 01 April 2024 Accepted: 13 August 2024 Published: 23 December 2024

ABSTRACT

During the manufacturing or processing of materials, large volumes of water of the required quality are often needed. Industrial water treatment and water purification is the process of removing impurities and pollution from the considered medium. To obtain liquid with specified quality parameters, complex systems of filters and treatment facilities are generally used. In this work, the cleaning process for a filtration column is studied. Three-dimensional numerical simulations of flow in a columnar array consisting of a porous medium are conducted. In particular, a model case corresponding to laboratory conditions is examined, with potassium salt being considered as a pollutant. It is assumed that the vertical column is a desalination system, as a result of which saturation and clogging of the pores of the medium occur; at the end of the operating cycle of such a filter, washing is required. Filtration modeling is implemented through the Brinkman approach taking into account density stratification. It is found that owing to density stratification and related effects, clean water moves in the central part of the filter, while contaminants near the side walls remain motionless for a long time. A solution to this problem is presented by changing the flow rate of supplied water.

KEYWORDS

Filtration column; binary mixture; Rayleigh-Taylor instability; Brinkman model

Nomenclature

ρ	Density of the liquid
v_i	Velocity vector
$i = x,\ y,\ z$	Cartesian coordinates
μ	Dynamic viscosity of the liquid
δ_{ij}	Kronecker symbol
m	Porosity of porous medium
K	Permeability of porous media
$\nabla = \partial/\partial x_i$	Nabla operator
$\mathbf{J}$	Vector of the diffusion flow of the impurity
D_m	Molecular diffusion coefficient
R	Cleaning coefficient
χ	Solutal expansion coefficient

1 Introduction

Analysis of concentration convection in order to find an effective way to control the filtration process during the transport of a limited volume of impurities in a porous column is in demand, since it is widely used on an industrial scale. A fairly large number of works have been carried out within the framework of laboratory experiments and theoretical studies of systems characterized by laboratory scales. However, most studies were carried out in a range of parameters for which gravitational effects were assumed to be insignificant [1–5]. Experimental and numerical studies of the control of convective flows in porous media are mostly devoted to thermal convection [6–10]. Some of the first works that considered the stability of convective motion in a porous medium are [11,12]. In these works, it was shown that in a layer of a porous medium, at a given temperature (concentration) difference between the boundaries, a flow in the form of convective cells, the width of which is equal to the depth of the layer, arises in a threshold manner. Later in [13], it was found that in the case of a pressure flow through a layer of a porous medium, the same flow occurs, but the amplitude of the velocity and concentration fluctuate around the average values, and the frequency of oscillations is proportional to the speed of the pressure flow.

When a liquid flows in an array of porous media, there is a problem of visualizing changes in the concentration of the solution spreading in the carrier medium. Laboratory-scale solute dispersion imaging experiments are performed on transparent model porous media of varying morphologies. This is how the coefficients of longitudinal and transverse dispersion are assessed depending on the liquid flow rate and the corresponding modes of dispersion of dissolved substances are determined [14–17].

A number of researchers have conducted laboratory experiments on the transport of contaminants in sand columns [18–21]. In [18,19] the authors studied the flow and mixing processes of waters of variable density in porous media in laboratory reservoir models and concluded that changes in density can create complex flow and mixing patterns. Numerical simulations of laboratory experiments performed in [20] using both conservative and reactive tracers under transient flow conditions in porous media and found that the numerical results were nearly identical to measured concentrations, and that transient flow enhanced lateral mixing and reaction controlled by stirring. The dynamics of sodium chloride (NaCl) and the food color brilliant blue FCF (BBF) through a column with homogeneous quartz sand is studied in [21]. It is found that sodium chloride behaves less differently and is not a passive impurity, which is characterized by complex convective regimes.

The remediation of contaminated water-saturated porous media has attracted widespread attention from many researchers and organizations [22]. The quality of consumed water, the development of which depends on the cleaning of porous media, is an important topic. The main problem arises when a permanent source is found in the groundwater from dissolved contamination [23]. Stable plumes are found in aquifers [24,25]. The long-term storage and slow release of contaminants from low-permeability water bodies (back diffusion) seriously impede aquifer restoration. Thus, pollutants from low-permeability zones are considered secondary sources of pollution after removal or isolation of primary sources [26]. Unfortunately, the removal of contaminants in areas of low permeability is difficult, and thus the process of back diffusion represents a potential limitation to aquifer restoration [27]. In [28], a series of experiments focused on evaluating dissolved contaminant flushing in cylindrical models containing a cylindrical low-conductivity zone is considered. The solute tailing in spatially heterogeneous porous media was studied. Analysis of a contaminant propagation from region of low-permeability was performed also in [29].

All mentioned above experimental work on the transport of solutes through water-saturated layers of porous media was performed for parameters of laboratory setup. For industrial installations characterized by dimensions on the order of ten meters, such studies have not been carried out in combination with a

changing hydrodynamic gradient caused by changing boundary conditions. Thus, more research is needed to fully understand the behavior of variable density water flow and solute transport as hydrodynamic gradients change. Since a visualized study of processes under industrial conditions is not possible, numerical simulation of the flow of water of variable density and the transport of dissolved substances (which are continuously injected) is carried out in the framework of this work under unsteady conditions in a homogeneous column of a porous medium. The objectives of this study were: (1) to evaluate the effect of a varying hydrodynamic gradient on the transport behavior of a dense sodium chloride solution in a homogeneous, open-ended, water-saturated column of a porous industrial tank; (2) to evaluate fluid flow and solute transport parameters; and (3) to investigate the transport behavior of sodium chloride in terms of spatiotemporal concentration distribution as well as the shape of convective structures to gain insight into transport mechanisms as hydrological parameters change.

2 Problem Statement

Mechanical water purification is required to comply with standard indicators of turbidity, transparency, and color due to the presence of insoluble suspended particles of sand, clay, silt, colloidal iron and silicon, pipeline rust, scale and other impurities. Mechanical purification is the most common method of water purification. A mechanical filter protects process equipment from clogging and premature failure at subsequent stages of cleaning. The filters, up to ten meters high, are often used to organize industrial water treatment (Fig. 1).

Figure 1: Industrial filter for mechanical cleaning called vertical filtration column

The operation of such filters usually includes the filter back-flushing stage, which is necessary to clean the filter from accumulated contaminants. To calculate the effective injection rate of clean water, three-dimensional numerical modeling of a vertical porous column is carried out, during which the emergence and development of convective flows in industrial filtration columns during the washing process are studied.

Three-dimensional numerical modeling of flow in a columnar displacement array consisting of a porous medium, characterized by spatial dimensions of industrial samples. In particular, the filtration column with diameter of 3.4 m and height of 7.8 m is considered. The vertical column is assumed to be a desalination system, as a result of which saturation and clogging of the pores of the medium occur. Thus, the potassium salt is considered as a pollutant in the present study.

The modeling is carried out based on the Brinkman equation of filtration taking into account density stratification. The finite volume method was used to discretize the governing equations and boundary conditions. For spatial discretization of the equations, the second-order accuracy scheme was used. The time evolution was modeled via an explicit second-order scheme.

3 Mathematical Model and Numerical Setup

The problem is solved within the framework of a non-stationary isothermal approach. The equations of filtration in tensor form are

$$\frac{\partial}{\partial t}(m\rho) + \nabla \cdot (\rho \vec{\mathrm{v}}) = 0 \tag{1}$$

$$\frac{\partial}{\partial t}\vec{\mathrm{v}} + \frac{1}{m^2}(\vec{\mathrm{v}} \cdot \nabla)\vec{\mathrm{v}} = -\frac{1}{\rho}\nabla p + \frac{\mu}{m\rho}\Delta\vec{\mathrm{v}} - \frac{\mu}{K}\vec{\mathrm{v}} + \rho\vec{g}, \tag{2}$$

where m, K are porosity and permeability of the porous medium, respectively; ρ is density of the liquid, v_i are components of the velocity vector (i = 1, 2, 3), μ is kinematic viscosity of the liquid.

The impurity transfer equation reads

$$\frac{\partial}{\partial t}(m\rho c) + \nabla \cdot (\rho \vec{\mathrm{v}} c) = -\nabla \cdot \vec{J}. \tag{3}$$

Here c is the dimensionless concentration of contaminants, $\vec{J}$ is the diffusion flux of the impurity, calculated by the expression

$$\vec{J} = -\rho D_m \nabla c, \tag{4}$$

where D_m is the specified molecular diffusion coefficient.

The geometry of the computational domain and the computational grid are shown in Fig. 2. On the solid walls of the computational domain, conditions of adhesion and impermeability to matter are set. At the inlet of the computational domain, a constant operating pressure and a constant impurity concentration equal to zero are specified. It was assumed that at the initial moment the filter was uniformly filled with impurities. At the outlet from the computational domain, normal atmospheric pressure is set. At other boundaries, the condition of adhesion is hold, and the boundaries are considered impermeable to filtration flow. The dependence of density on concentration is specified by the following formula [30]:

$$\rho = \rho_0 + \chi c \tag{5}$$

where $\rho_0 = 999.993\ \mathrm{kg/m^3}$ is the density of pure water, $\chi = \partial\rho/\partial c$ is the coefficient describing the concentration caused change of density. We assume that $\chi = 250$ g/l and the initial state corresponds to $c = 1$, so the initial concentration equals to the concentration of a saturated solution of 250 g/l. The inlet pressure is varied from 1 to 20 atm in order to study the effect of pumping on the backflushing efficiency.

Calculations are carried out using ANSYS Fluent software, which implements the finite volume method. The spatial discretization is performed using the third-order MUSCL scheme (Monotone Upstream-Centered Schemes for Conservation Laws). The gradients are computed according to the least squares cell-based method that assumes the solution to vary linearly over a cell. The method is less computational expensive than the node-based gradient algorithm, while provide similar accuracy. The pressure-based coupled solver is used for simulations, which allows to obtain a robust solution using considerably larger time steps compared to the segregated solution schemes. Condition of zero normal velocity is hold at solid boundaries and condition on pressure is implemented for the inlet and the outlet. It is assumed that pure water is flowing in at the inlet.

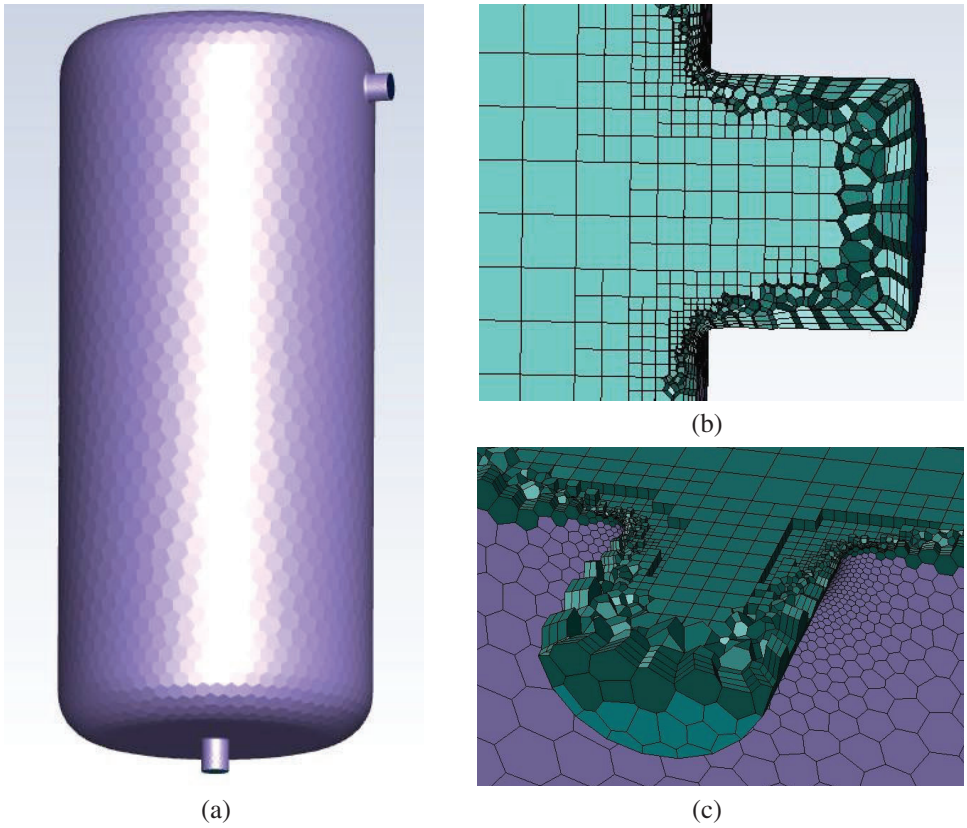

Figure 2: Geometry of the computational domain (a) and the computational mesh near the outlet (b) and the inlet (c)

The time evolution is modeled using second-order scheme. The time step is determined by stability criteria according to the adaptive time stepping algorithm. Based on an evaluation of the truncation error related to the time integration scheme, the time step size is automatically determined. The size of the time step is increased if the truncation error is less than a given tolerance, and decreased if the truncation error is larger. An algorithm of the predictor-corrector type is used by ANSYS Fluent to estimate the truncation error [31]. In our calculation, the time step was approximately equal to $2 \cdot 10^{-3}$ s. At each time step the convergence criterion for the velocity components is used. The relative residual errors have to be less than 0.001.

The computational mesh consisting of rectangular cells for internal volume and quadrangular or pentagonal prisms near solid boundaries was used (see Fig. 2). To perform the mesh convergence analysis and select the spatial mesh step, calculations were carried out for three different grids (see Table 1). The change in concentration shows that the results for the 0.075 m grid differ from the results obtained for the 0.01 and 0.075 m grids by more than 5%. For grids characterized by steps of 0.05 m and 0.025, the difference in the maximum concentration is less than 2%. Therefore, the mesh with the step of 0.05 m was used to carry out computational experiments (the number of mesh nodes is 1.5 million).

4 Mathematical Model Verification

The verification case suggested in [32] was used to verify the implemented mathematical model of transport in porous media. It considers a domain containing two zones of different porosities and permeabilities. In particular, the 10 m long, one-dimensional area is split into two equal sections. One

half is free water (porosity had porosity of 1), while the other half is made up of soil (had porosity of 0.3, which is equivalent to a 0.01 m effective particle diameter). At the entrance of the computing area, a continuous flow is established using the passive impurity concentration as an indicator. A fixed intake flow rate of 0.01 m/s is used. The calculation area is initially filled with impurity-free, clean water.

Table 1: Dependence of maximum impurity concentration, C, at the outlet on the mesh spatial mesh step, D, for flushing pressure of 2 atm and t = 500 s

D, m	0.075	0.05	0.01
C	0.28	0.321	0.314

We compared the outcomes of our simulation with known analytical solution for this one-dimensional continuous injection problem (see [32]). The simulated curves obtained under continual injection show a good agreement with the analytical results, as shown in Fig. 3. As one can see, the concentration front moves across the medium nearly without affecting its structure.

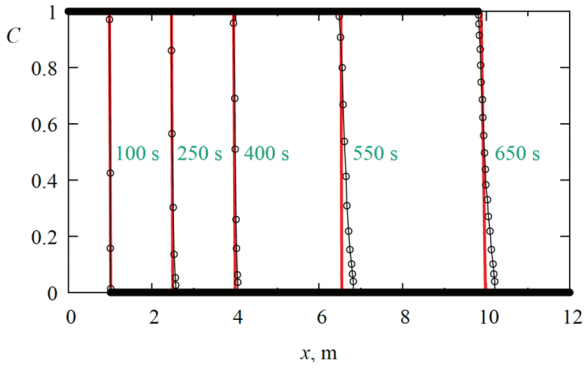

Figure 3: Comparison between simulation result (points) and the analytical solution (lines)

5 Modeling Results

Numerical modeling revealed that at low operating flushing pressures, the development of Rayleigh-Taylor instability occurred. Fig. 4 shows the evolution of the impurity concentration in the vertical section of the filter and the flow line (fluid trajectory) at a flushing pressure of 2 atm. Initially the field of filtration velocity is nearly uniform with a magnitude of 0.012 m/s (Fig. 4a). Then, density stratification effects cause clean water to move in the central part of the filter, while contaminants near the side walls remain stationary for a long period of time (Fig. 4b). Similar behavior was observed in simulations performed in [33]. In addition, the development of the Rayleigh-Taylor instability causes the appearance of vortex flows in the upper part of the filter (see Fig. 4b). All this leads to a decrease in washing efficiency: a significant part of the impurity remains near the filter walls for a long time during washing.

At high flushing rates, the Rayleigh-Taylor instability does not have time to develop, and the impurity is completely displaced from the porous medium. Fig. 5 shows the washing process at a pressure of 20 atm. At the beginning of the back-flushing process the displacement front has the shape of a hemisphere (see Fig. 5a), then, it becomes almost flat (see Fig. 5b). The velocity field remains nearly uniform with a magnitude of 0.076 m/s. In this case, the impurity is completely displaced near the side surface of the filter.

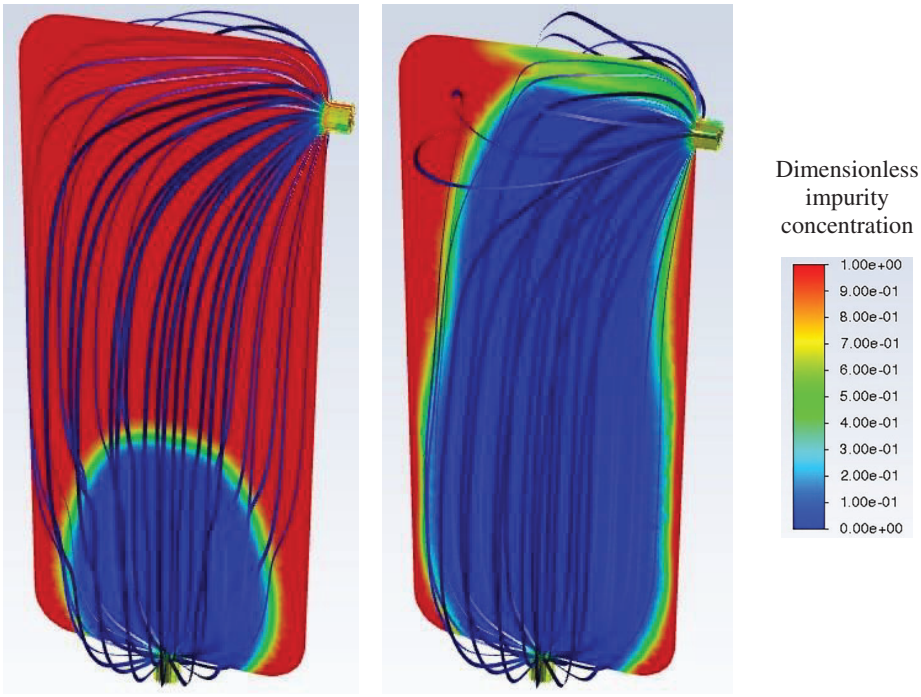

Figure 4: Concentration of impurities in the vertical section and fluid flow trajectories at a flushing pressure of 2 atm. At different times: (a) t = 100 s, (b) t = 500 s

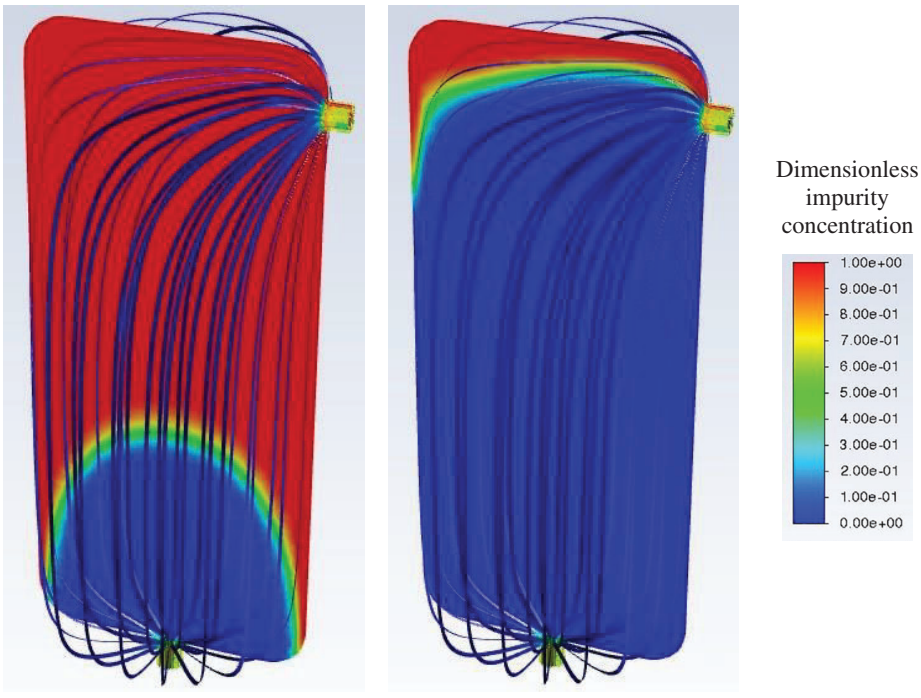

Figure 5: Concentration of impurities in the vertical section and fluid flow trajectories at a flushing pressure of 20 atm. at different times: (a) t = 10 s, (b) t = 50 s

The dependence of the washing efficiency can be accessed via the filter cleaning coefficient, which is calculated according to the formula:

$$R = \int \frac{\rho_1 - \rho_r}{\rho_1 - \rho_0} dV \cdot 100\%, \tag{6}$$

where integration is performed over the filter volume, ρ_r is the residual density of the mixture, ρ_0 is the density of pure water, ρ_1 is the density of the saturated solution which corresponds to $C = 1$. This coefficient characterizes the amount of the impurity washed off during the flushing.

Fig. 6 shows the dependence of the cleaning coefficient on the flushing pressure, calculated for a cleaning time of 10 min. As can be seen, this dependence is nonlinear. At low flushing pressures, efficiency is greatly reduced. At high flushing pressures, the Rayleigh-Taylor instability does not have a significant effect on the flushing process and the impurity is almost completely displaced from the filter. As shown in Fig. 6, the numerical modeling reveals that the inlet pressure between 9 and 13 atm results in the flushing efficiency of only 85% after 10 min (approximately 15% residual impurities remain in the filter). With further increase of flushing pressure, the efficiency substantially improves. The pressure exceeding 18 atm allows for 100% cleaning of the filtration column.

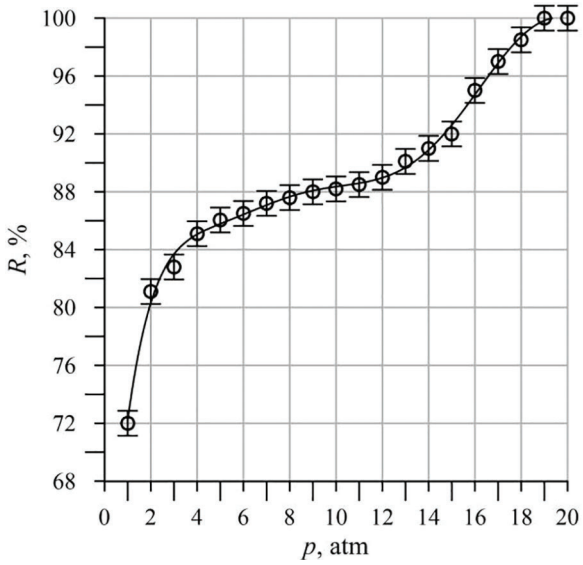

Figure 6: Dependence of the filter cleaning coefficient on the operating pressure

It is worth to note that the Rayleigh-Taylor instability develops though a bifurcation in this process. Initially the density stratification is stable, but during the flushing, as the front of the impurity displacement moves upward, the unstable stratification forms and the instability starts to develop. In that case, variation of the calculation's parameters may influence not only of the rate of the Rayleigh-Taylor instability development but also on the time then it appears. As a result, one can expect some variation of the calculated values with rather small changing of the inlet pressure. To estimate the calculation error, the modelling was repeated with small increase and decrease in the inlet pressure (in particular +100, +50, −50, −100 Pa). Then, the error estimation was performed by conventional technique. At first, the mean value and the standard deviation were calculated. Further, the confidence limits, shown in Fig. 6, were calculated by multiplying the standard deviation and the Student coefficient for confidence probability 99.7% (3σ).

6 Discussion

Under gravity, when liquids of different densities are arranged in a porous medium so that the heavier liquid is above the lighter one, any small disturbance at the boundary leads to the emergence of instability, which has the form of non-stationary growth of finger structures. This Rayleigh-Taylor instability develops in such a way that disturbances at the boundary grow exponentially with time. Such dynamics are predicted by the linearized Rayleigh-Taylor theory, but at finite times nonlinear effects occur and the dynamics change. Rayleigh-Taylor instability can occur at different length scales, which depends not only on the size of the system, but also on external influences and flows. This explains some effects of cloud formation in meteorology [34] and the formation of finger-like structures in astrophysics [35]. In the review by Kelly et al. [36] the influence of flows on the shape of the resulting currents is shown. Scaling of Rayleigh-Taylor mixing in porous media was considered in [37]. In our case, we consider an incoming flow of a less dense liquid into a denser one. In this case, finger instability is not observed; a vortex of the order of the horizontal dimensions of the system arises, leading to the emergence of a residual concentration during the filter washing process. A similar liquid flow was observed in [33] when considering the wave profile of the initial disturbance for two mixing liquids, and in [37], where the numerical simulation show that the balance between gravity and viscous forces can result in a growth of elongated plumes.

7 Conclusion

Three-dimensional numerical modeling of flow in a columnar displacement array consisting of a porous medium characterized by the spatial dimensions of industrial samples was carried out. A model case corresponding to laboratory conditions was considered when potassium salt was taken as a pollutant while the size of the column corresponded to the industrial scales. Thus, it is assumed that the vertical column is a desalination system, where saturation and clogging of the pores of the medium occur. Therefore, at the end of the filter's operating cycle, it must be washed. Filtration modeling was carried out on the basis of the Brinkman model, taking into account density stratification. ANSYS Fluent, which implements the finite volume method to discretize the governing equations and boundary conditions, was used to carry out the modeling.

Numerical modeling revealed that at low operating flushing pressures, the development of Rayleigh-Taylor instability is observed. The evolution of the impurity concentration in the vertical section of the filter was monitored, and streamlines (fluid trajectories) were plotted for different flushing pressures. It is found that the effects of density stratification cause clean water to be moved up only in the central part of the filter, while contaminants near the side walls remain motionless for a long time. In addition, the development of the Rayleigh-Taylor instability causes vortex flows to appear in the upper part of the filter. All this leads to a decrease in washing efficiency because a significant part of the impurity remains near the filter walls during washing. During the flushing process at a pressure of 20 atmospheres, at the initial moments, the displacement front has the shape of a hemisphere, and then it becomes almost flat. In this case, the impurity is completely displaced near the side walls of the filter.

The efficiency of washing is analyzed by the dependence of the filter cleaning coefficient on the operating pressure at the inlet of the filtration column. It is shown that this dependence is nonlinear, and efficiency is greatly reduced at low flushing pressures. When flushing pressures exceed 18 atm, the Rayleigh-Taylor instability does not have time to develop, and the impurity can be almost completely removed from the filter.

Acknowledgement: Computations were performed on the Uran supercomputer at the IMM UB RAS.

Funding Statement: The research was supported by a grant from the Russian Science Foundation (Project No. 20-11-20125).

Author Contributions: The authors confirm contribution to the paper as follows: study conception and design: Yanina N. Parshakova, Andrey Ivantsov; data collection: Andrey Ivantsov; analysis and interpretation of results: Yanina N. Parshakova, Andrey Ivantsov; draft manuscript preparation: Yanina N. Parshakova. All authors reviewed the results and approved the final version of the manuscript.

Availability of Data and Materials: The data presented in this study are available on request from the corresponding author.

Ethics Approval: Not applicable.

Conflicts of Interest: The authors declare no conflicts of interest to report regarding the present study.

References

1. Pang L, Close M, Greenfield H, Stanton G. Adsorption and transport of cadmium and rhodamine WT in pumice sand columns. N Z J Mar Freshwater Res. 2004;38:367–78. doi:10.1080/00288330.2004.9517244.
2. Gouze P, Le Borgne T, Leprovost R, Lods G, Poidras T, Pezard P. Non-Fickian dispersion in porous media: 1. Multiscale measurements using single-well injection withdrawal tracer tests. Water Resour Res. 2008;44(6):1759. doi:10.1029/2007WR006278.
3. Agaoglu B, Scheytt T, Copty NK. Laboratory-scale experiments and numerical modeling of cosolvent flushing of multi-component NAPLs in saturated porous media. J Contam Hydrol. 2012;140:80–94. doi:10.1016/j.jconhyd.2012.07.005.
4. Lu B, Zhang Y, Zheng C, Green CT, O'Neill C, Sun HG, et al. Comparison of time nonlocal transport models for characterizing non-fickian transport: from mathematical interpretation to laboratory application. Water. 2018;10(6):778. doi:10.3390/w10060778.
5. Parshakova Y, Ivantsov A. Dynamics of pollution in the hyporheic zone during industrial processing brine discharge. Water. 2022;14(24):4006. doi:10.3390/w14244006.
6. Kaneko T, Mohtadi MF, Aziz K. An experimental study of natural convection in inclined porous media. Int J Heat Mass Transf. 1974;17(4):485–96. doi:10.1016/0017-9310(74)90025-8.
7. Jiang PX, Xu YJ, Lv J, Shi RF, He S, Jackson JD. Experimental investigation of convection heat transfer of CO_2 at super-critical pressures in vertical mini-tubes and in porous media. Appl Therm Eng. 2004;24(8):1255–70. doi:10.1016/j.applthermaleng.2003.12.024.
8. Sommer O, Heiland H, Wozniak G. Experimental investigation of thermal convection in an inclined gap. PAMM. 2012;12(1):479–80. doi:10.1002/pamm.201210228.
9. Abdelkrim L, Djezzar M. Convective heat and solute transfer in Newtonian fluid saturated inclined porous cavity. Int J Phys Res. 2014;2:78. doi:10.14419/ijpr.v2i2.3372.
10. Doğan A, Ozbalci O, Atmaca I. Experimental investigation of natural convection from porous blocks in a cavity. J Porous Media. 2016;19:1023–32. doi:10.1615/JPorMedia.v19.i12.10.
11. Horton CW, Rogers FT. Convection currents in a porous medium. J Appl Phys. 1945;16(6):367–70. doi:10.1063/1.1707601.
12. Lapwood ER. Convection of a fluid in a porous medium. Math Proc Camb Philos Soc. 1948;44(4):508–21. doi:10.1017/S030500410002452X.
13. Prats M. The effect of horizontal fluid flow on thermally induced convection currents in porous mediums. J Geophys Res. 1966;71(20):4835–8. doi:10.1029/JZ071i020p04835.
14. Charlaix E, Hulin JP, Leroy C, Zarcone C. Experimental study of tracer dispersion in flow through two-dimensional networks of etched capillaries. J Phys D: Appl Phys. 1988;21(12):1727. doi:10.1088/0022-3727/21/12/010.
15. Detwiler RL, Rajaram H, Glass RJ. Solute transport in variable-aperture fractures: an investigation of the relative importance of Taylor dispersion and macrodispersion. Water Resour Res. 2000;36(7):1611–25. doi:10.1029/2000WR900036.

16. Theodoropoulou MA, Karoutsos V, Kaspiris C, Tsakiroglou CD. A new visualization technique for the study of solute dispersion in model porous media. J Hydrol. 2003;274(1):176–97. doi:10.1016/S0022-1694(02)00421-3.
17. Tsakiroglou C, Theodoropoulou M, Karoutsos V, Papanicolaou D. Determination of the effective transport coefficients of pore networks from transient immiscible and miscible displacement experiments. Water Resour Res. 2005;41(2):W02014. doi:10.1029/2003WR002987.
18. Schincariol RA, Schwartz FW. An experimental investigation of variable density flow and mixing in homogeneous and heterogeneous media. Water Resour Res. 1990;26(10):2317–29. doi:10.1029/WR026I010P02317.
19. Swartz CH, Schwartz WF. An experimental study of mixing and instability development in variable-density systems. J Contam Hydrol. 1998;34(3):169–89. doi:10.1016/S0169-7722(98)00088-6.
20. Rolle M, Eberhardt C, Chiogna G, Cirpka OA, Grathwohl P. Enhancement of dilution and transverse reactive mixing in porous media: experiments and model-based interpretation. J Contam Hydrol. 2009;110(3):130–42. doi:10.1016/j.jconhyd.2009.10.003.
21. Qian J, Wu Y, Zhang Y, Liu Y, Lu Y, Yu Z. Evaluating differences in transport behavior of Sodium Chloride and brilliant blue FCF in sand columns. Transp Porous Media. 2015;109. doi:10.1007/s11242-015-0551-40.
22. Gao H, Tatomir AB, Karadimitriou NK, Steeb H, Sauter M. Effect of pore space stagnant zones on interphase mass transfer in porous media, for two-phase flow conditions. Transp Porous Media. 2023;146:639–67. doi:10.1007/s11242-022-01879-0.
23. Ding XH, Feng SJ, Zheng QT. Forward and back diffusion of reactive contaminants through multi-layer low permeability sediments. Water Res. 2022;222:118925. doi:10.1016/j.watres.2022.118925.
24. Li Z, Qiu Y, Zhao D, Li J, Li G, Jia H. Application of apatite particles for remediation of contaminated soil and groundwater: a review and perspectives. Sci Total Environ. 2023;904:166918. doi:10.1016/j.scitotenv.2023.166918.
25. You X, Liu S, Dai C, Guo Y, Zhong G, Duan Y. Contaminant occurrence and migration between high-and low-permeability zones in groundwater systems: a review. Sci Total Environ. 2020;743:140703. doi:10.1016/j.scitotenv.2020.140703.
26. Blue J, Boving T, Tuccillo ME, Koplos J, Rose J, Brook M, et al. Contaminant back diffusion from low-conductivity matrices: case study of remedial strategies. Water. 2023;15:570. doi:10.3390/w15030570.
27. Borden RC, Cha KY. Evaluating the impact of back-diffusion on groundwater cleanup time. J Contam Hydrol. 2021;243:103889. doi:10.1016/j.jconhyd.2021.103889.
28. Kurawasa T, Takanashi Y, Suzuki M, Inoue K. Laboratory flushing tests of dissolved contaminants in heterogeneous porous media with low-conductivity zones. Water, Air, Soil Poll. 2023;234:240. doi:10.1007/s11270-023-06236-5.
29. Viotti P, Luciano A, Mancini G, Tatti F. Lab investigation using a box model and image analysis of a contaminant back-diffusion process from low-permeability layers. Sustainability. 2023;15:16950. doi:10.3390/su152416950.
30. Millero FJ, Poisson A. International one-atmosphere equation of state of seawater. Deep Sea Res Part A. Oceanographic Res Papers. 1981;28(6):625–9. doi:10.1016/0198-0149(81)90122-9.
31. Gresho PM, Lee RL, Sani RL. On the time-dependent solution of the incompressible navier-stokes equations in two and three dimensionson the time-dependent solution of the incompressible navier-stokes equations in two and three dimensions. In: Recent advances in numerical methods in fluids. Swansea, UK: Pineridge Press; 1980.
32. Broecker T, Gollo VS, Fox A, Lewandowski J, Nützmann G, Arnon S, et al. High-resolution integrated transport model for studying surface water-groundwater interaction. Groundwater. 2021;59:488–502. doi:10.1111/gwat.13071.
33. Forbes LK, Browne CA, Walters SJ. The Rayleigh-Taylor instability in a porous medium. Discover Appl Sci. 2021;3:188. doi:10.1007/s42452-021-04160-z.
34. Boffetta G, Mazzino A. Incompressible Rayleigh-Taylor turbulence. Annu Rev Fluid Mech. 2017;49:119–43. doi:10.1146/annurev-fluid-010816-060111.

35. Hester JJ. The Crab Nebula: an astrophysical chimera. Annu Rev Astron Astrophys. 2008;46:127–55. doi:10.1146/annurev.astro.45.051806.110608.
36. Kelley MC, Dao E, Kuranz C, Stenbaek-Nielsen H. Similarity of Rayleigh-Taylor instability development on scales from 1 mm to one light year. Int J Astron Astrophys. 2011;1:173–6. doi:10.4236/ijaa.2011.14022.
37. Boffetta G, Borgnino M, Musacchio S. Scaling of Rayleigh-Taylor mixing in porous media. Phys Rev Fluids. 2020;5:62501. doi:10.1103/PhysRevFluids.5.062501.